Grain structure evolution during cryogenic rolling of alpha brass

T. Konkova[a], S. Mironov[a,b], A. Korznikov[a,c], G. Korznikova[a], M.M. Myshlyaev[d], S.L. Semiatin

[a]Institute for Metals Superplasticity Problems, Russian Academy of Science, Ufa 450001, Russia
[b]Institute for Metals Superplasticity Problems, Russian Academy of Science, Ufa 450001, Russia; and Department of Materials Processing, Graduate School of Engineering, Tohoku University, Sendai 980-8579, Japan
[c]National Research Tomsk State University, Tomsk 634050, Russia
[d]Baikov Institute of Metallurgy and Material Science, Russian Academy of Science, Moscow 119991, Russia; and Institute of Solid State Physics, Russian Academy of Sciences, Chernogolovka, Moscow oblast 142432, Russia
[e]Air Force Research Laboratory, Materials and Manufacturing Directorate, AFRL/RXCM, Wright-Patterson AFB, Ohio 45433-7817, USA

High-resolution electron backscatter diffraction (EBSD) was used to study grain structure development during cryogenic rolling of Cu–29.5Zn brass. Microstructure evolution was found to be broadly similar to that occurring during rolling at room temperature. Specifically, favorably-oriented grains (Copper {112}<111> and S {123}<634>) experienced profuse deformation twinning followed by extensive shear banding. This eventually produced an ultrafine structure with a mean grain size of 0.2 μm. On the other hand, grains with crystallographic orientations close to Brass {110}<112> and Goss {110}<100> were found to be stable against twinning/shear banding and thus showed no significant grain refinement. As a result, the final structure developed in heavily-rolled material was distinctly inhomogeneous consisting of mm-scale remnants of original grains with poorly developed substructure and ultra-fine grain domains.

Keywords:

Nanostructured materials
Nanofabrication
Grain boundaries
Microstructure
Scanning electron microscopy

1. Introduction

Large deformation at cryogenic temperatures is sometimes considered as a promising cost-effective method for producing bulk ultra-fine grain materials [e.g. 1–12]. To date, the majority of research in the field of cryogenic working has focused on aluminum and copper alloys, most likely because of the superior ductility of these materials [1,2,4–10]. It has been established that the key mechanism governing grain-structure evolution in both materials at cryogenic temperatures is the geometrical effect of strain

per se [1,2]. In other words, grains change their shape in proportion to the imposed strain, and noticeable grain subdivision and mechanical twinning are not observed [1,2]. By this means, a reasonably homogeneous grain structure, dominated by heavily elongated grains aligned with the direction of macroscopic material flow, is developed [1,2]. Such grain structures typically contain a significant proportion of low-angle boundaries [1,2] and, in the case of copper, a high density of free dislocations [2]. The limited formation of deformation-induced boundaries during cryogenic deformation is believed to be partially associated with suppression of cross-slip at low temperatures [2]. This effect is also responsible for the strengthening of the {110}<112> Brass texture in cryorolled materials [1,2].

On the other hand, pronounced microstructural refinement has been observed during cryogenic deformation of commercial-purity titanium [3] and alpha brass [11,12]. In these materials, the formation of nano-scale structure has been reported and this effect has been essentially attributed to extensive mechanical twinning and shear banding [3,11,12]. Thus, it appears that cryogenic deformation is most effective in materials prone to activation of these two deformation mechanisms.

Due to its very low stacking fault energy, extensive twinning and shear banding usually occur during cold deformation of Cu– 30Zn brass, and thus significant grain refinement may be expected. This effect is well documented for rolling of this material at ambient temperature [13]. Because dislocations in this alloy are dissociated into partials, a distinct cell structure is not developed [13]. This gives rise to significant strain hardening and thus activates profuse deformation twinning after 50 pct. of reduction [13]. Furthermore, twinning develops very heterogeneously. The twins concentrate preferentially in grains with crystallographic orientations close to Copper {112}<111> and S {123}<634>, whereas Goss {110}<100> and Brass {110}<112> orientations are typically twin-free [13]. The extensive twinning produces a nano-scale lamellar-like twin-matrix structure [13]. Due to the very small slip distance, subsequent slip in the twinned areas occurs primarily along a common twin/matrix {111} plane [13]. This provides a rotation of the slip plane toward rolling plane, thus leading to the formation of the a {111}<uvw> c-fiber texture and a reduction in the associated Schmid factor for slip to zero [13]. Simultaneously, alternate octahedral slip planes undergo latent hardening. Thus, after 50–60% thickness reduction, the twins are strongly aligned, and intense shear banding occurs as a result of the suppression of grain-scale slip [13]. The crystallographic orientations within the shear bands are widely scattered but show a certain preference for Goss {110}<100> and Brass {110}<112> texture components [13]. The shear bands consist of very fine (0.1 μm) crystallites [13].

It may be hypothesized that the pronounced grain-refinement effect observed during rolling of Cu–30Zn brass at room temperature may be enhanced at cryogenic temperatures. The first studies in this area confirmed the development of extensive twinning eventually leading to the formation of a nano-scale structure [14–16]. It should be noted however that the microstructure observations in these works were performed primarily by transmission electron microscopy (TEM). Despite the excellent resolution of TEM, the statistical reliability of such results is not clear. Hence, the objective of the present work was to provide deeper insight into the mechanisms of grain refinement and texture evolution during cryogenic rolling of alpha brass using electron back-scatter diffraction (EBSD) imaging.

2. Material and experimental procedures

The program material comprised alpha brass, with a measured composition (in wt.%) of 29.5 Zn, 0.5 Pb and balance Cu. The material was manufactured by ingot casting. In an attempt to recrystallize it prior to cryogenic rolling, the material was cold rolled to a 10% thickness reduction and subsequently annealed at 800 C for 30 min. However, recrystallization was not complete, and the resulting material contained a significant fraction of retained millimeter-size dendritic grains (Supplementary data, Fig. S1).

The material was cryogenically rolled to 90 pct. overall thickness reduction (true strain = 2.3) using a reduction per pass of 10 pct. In order to provide cryogenic deformation conditions, the rolling perform and work rolls were soaked in liquid nitrogen prior to each pass and held for 20 min; immediately after each pass, the workpiece was re-inserted into liquid nitrogen. The typical flat-rolling convention was adopted in this work; i.e. the rolling, long-transverse, and thickness/normal directions were denoted as RD, TD, and ND, respectively.

To preserve the deformation-induced microstructure, the cryo-rolled material was stored in a freezer at 20 C prior to examination.

Microstructure characterization was performed primarily via EBSD examination of the mid-thickness rolling plane (containing the RD and TD). For this purpose, samples were prepared using conventional metallographic techniques followed by long-term (24 h) vibratory polishing with a colloidal-silica suspension. EBSD analysis was conducted with a JSM-7800F field-emission-gun, scanning-electron microscope (FEG-SEM) equipped with a TSL OIM™ EBSD system. To examine microstructure at different scales, several EBSD maps were acquired in each sample with a scan step size ranging from 2 to 0.05 μm. To improve the reliability of the EBSD data, small grains comprising three or fewer pixels were automatically removed from the maps using the grain-dilation option in the TSL software. Furthermore, to eliminate spurious boundaries caused by orientation noise, a lower limit boundary-misorientation cutoff of 2^{o} was used. A 15^{o} criterion was employed to differentiate low-angle boundaries (LABs) and high-angle boundaries (HABs).

To obtain a broader view of deformation and underlying microstructure changes, the Vickers microhardness was also measured on each sample at ambient temperature using a load of 100 g for 10 s. At least 25 measurements were made in each case to obtain an average value.

Because of the very large initial grain size, there was substantial variation in the deformed microstructures throughout the samples. This made quantitative evaluation of the typical microstructure and texture parameters difficult, and, consequently, qualitative microstructure and texture trends are shown in the present paper.

3. Results and discussion

3.1. Broad aspects of deformation and grain structure evolution

The program material showed a high level of strain hardening as evidenced by the dependence of microhardness on true thickness strain (Fig. 1a). The microhardness was approximately tripled after a true strain of 1, thus indirectly suggesting major microstructural changes. However, at strains larger 1, the microhardness tended to saturate (Fig. 1a) and the hardening rate approached to zero (Fig. 1b). This latter seemed to indicate a stabilization of the strain-induced microstructure.

Several different types of EBSD data (i.e., orientation maps,[1]Kikuchi-band-contrast maps, and grain-boundary maps) provided insight into the microstructures developed after different levels of reduction (Figs. 2–5). For example, after a 10-pct. reduction (true strain 0.1), the original coarse-grained microstructure at low magnifications appeared to be almost unchanged (Fig. 2a). The sole exception to this observation was splitting of a few sporadic grains (circled in Fig. 2a). On the other hand, closer inspection of the microstructure at higher magnifications revealed evidence of substructure development. In the Kikuchi-band-contrast map (Fig. 2b), for example, the substructure appeared as alternating dark and bright bands aligned with traces of a {111} plane. In addition, the misorientations across the subboundaries were well below the EBSD detection limit of 2^o (Fig. 2c).

After a reduction to 30 pct. (true strain ≈ 0.4), there was extensive formation of deformation-induced boundaries, and their misorientations increased (Fig. 3a). Simultaneously, profuse twinning was observed in some grains[2] (Fig. 3b and c). This agrees well with prior TEM observations of cryo-rolled brass [14–16]. Therefore, an onset of the profuse twinning during cryogenic rolling seems to be shifted to lower strains as compared to rolling at room temperature (≈ 50 pct. reduction [13]). Remarkably, the deformation-induced LABs tended to cluster in the twinned areas, and thus the microstructure became noticeably inhomogeneous (Fig. 3a). As expected, the twins had a lenticular morphology and formed packages of narrow twin/matrix lamellae aligned with {111} planes (Fig. 3b and c).

After 50-pct. reduction, the LABs and twin substructure became much denser (Fig. 4a). The microstructure heterogeneity became more pronounced as well. Closer inspection of the twinned grains revealed extensive shear banding[3] (dark bands in Kikuchi-band contrast map in Fig. 4b). The shear bands typically comprised fine, highly-misoriented grains (an example is circled in Fig. 4c). Thus, the shear banding during cryogenic rolling also seems to be activated earlier that that during rolling at ambient temperature (≈ 60 pct. reduction [13]).

Further increase of thickness reduction to 90 pct. (true strain ≈ 2.3) resulted in no major changes in microstructure (Fig. 5). Specifically, the final microstructure was markedly inhomogeneous and still could be described in terms of remnants of coarse original grains with poorly developed substructure (‘‘stagnant grains’’) and ultra-fine grain domains located in previously twinned areas (Fig. 5a). The latter regions consisted of twins, shear bands, and LAB substructure (Fig. 5b and c). The observed microstructure stabilization agrees well with the revealed saturation of the microhardness at high levels of reduction (Fig. 1).

Per the microstructural observations, the grain refinement process was primarily attributable to deformation twinning and shear banding. Considering the importance of these two mechanisms, they are analyzed in more detail in the following two sections.

3.2. Twinning

To provide fundamental insight into twinning, the crystallographic orientations of the twinned areas were extracted from EBSD maps and plotted as orientation distribution functions (ODFs) (Fig. 6). At relatively low strains, the ODF was dominated by the Copper {112}<111>, S {123}<634>, and Twinned Copper{255}<511> orientations (Fig. 6a). This result was as expected because the orientations between the Copper and S[3] components are characterized by the highest twinning/slip Schmid-factor ratio [13]. At

[1] To see figures in color, a reader is referred to online version of this paper.

[2] The first (sporadic) twins were found after 20-pct. reduction (true strain of 0.2).

[3] The first (sporadic) shear bands were found after 30-pct. reduction (true strain of 0.4).

[3] Twinning of the S orientation leads exactly to the symmetrical equivalent variant and thus it does not produce an additional peak in the ODF [13].

larger strains, however, the {111}<uvw> γ fiber with a pronounced Y {111}<112> orientation became prevalent (Fig. 6b). This observation is also in the line with texture measurements for brass rolled at ambient temperature and may be attributed to crystallographic rotations of twinned Copper and S grains during subsequent slip [13,17]. Specifically, the Y {111}<112> orientation is believed to originate from the Twinned Copper {255}<511> orientation [13]. It seems therefore that the twinning mechanism is essentially the same at ambient and cryogenic temperatures.

To obtain additional insight into the twinning process, misorientation-angle distributions were derived from the twinned areas and analyzed (Fig. 7a). These results indicated that the twin induced peak near 60^o increased continuously with strain. This finding suggested that twinning continued for the entire range of strains that was investigated. Another interesting result was the substantial increase in LAB area with strain, particularly in the range of misorientations between 5 ^{o} and 15^o. This effect was most pronounced after 50 pct. reduction and was thus likely attributable to shear banding, as discussed in Section 3.1. Shear banding is wellknown to lead to considerable crystallographic rotations. As a result, the sheared twin boundaries may deviate from the ideal Σ3 relationship and even transform into random HABs [18]. To track this effect, misorientation perturbations along the twin boundaries (within the Brandon interval) were systematically measured for different rolling reductions (Fig. 7b). At low strains, the perturbations from the ideal twin/matrix relationship were small, typically being within the angular resolution of conventional EBSD. After the initiation of shear banding, however, the measured misorientations deviated significantly from Σ3 thus reflecting gradual destruction of the twin boundaries. The transformation of the structure of twin boundaries during cryo-rolling of brass has been recently confirmed by high-resolution TEM observations [15,16]. In a view of this effect, the observed enlargement of twin boundary area (Fig. 7a) supports the conclusion that twinning increased with strain.

3.3. Shear banding

The ODFs calculated for shear bands evolved after moderate and high strains are shown in Fig. 8. To a first approximation, the ODFs in both cases could be described primarily in the terms of the superposition of Y {111}<112>, Z {111}<110>, Goss {110}<100>, and Brass {110}<112> orientations. Again, this is in the line with texture measurements for brass rolled at room temperature [13,19–21]. The Y and Z orientations are well accepted to originate from twinning of Copper {112}<111> and S {123}<634> components and subsequent slip [13]. For the Y and Z orientations, slip is believed to become increasingly difficult with increasing strain because the Schmid factor for slip on the operative plane decreases toward zero and the slip distance for slip on the other {111} planes is limited by nano-scale twin/matrix lamellae [13]. This induces shear banding which rotates the Y and Z orientations toward the Goss orientation, and subsequent slip in the Goss produces the final stable Brass texture [13]. Thus, the presence of the Y, Z, Goss, and Brass orientations within the shear bands revealed in this work reflected different stages of texture development within shear bands. Therefore, it appears that the shear banding mechanism at cryogenic temperatures was broadly similar to that operating at ambient temperature.

The considerable crystallographic reorientations within the shear bands were accompanied by significant changes in the misorientation distribution (Fig. 9a). As expected, the twin-induced peak near 60^o was reduced significantly. Additionally, the low-angle part of distribution was moved to higher misorientations, thus reflecting extensive LAB-to-HAB transformation. This gave rise to an ultra-fine grained structure within the bands with a mean grain size of 0.2 μm.

It is important to point out that the mean grain size measured by EBSD in the present study is substantially coarser than that usually found in severely cold (or cryo-) rolled material by TEM [13,15,16]. This discrepancy may be associated with the very limited statistics of TEM measurements as well as with the relatively coarse EBSD scan step size used in this work which may have led to missing very small grains.

Remarkably, the volume fraction of the shear-banded area increased only slightly with strain (Fig. 9b). This may indicate that the shear bands were difficult to form, but once created they were relatively soft for subsequent slip.

3.4. Large remnant grains

A characteristic feature of the heavily-rolled material was the presence of a significant proportion of grains with poorly developed substructure (Figs. 4a and 5a). To ascertain the ‘‘stagnant’’ nature of these grains, their specific crystallographic orientations were determined (Fig. 10). The measured ODFs were found to be dominated by Brass {110}<112> and sometimes Goss {110}<100> orientations. These are characterized by the lowest twinning/slip Schmid-factor ratio (0.77 and 0.55, respectively) [13]. As a result, almost no twinning occurred in these grains despite cryogenic-deformation conditions [13]. Moreover, the formation of deformation-induced dislocation boundaries in these grains was probably difficult because of the low stacking fault energy of alpha brass as well as the reduced thermal activation at cryogenic temperature which would suppress climb, cross slip, and the related reorganization of dislocations into sub-boundaries [22]. In other words, the normal grain-subdivision processes associated with the development of deformation-induced dislocation boundaries were inhibited, and, therefore, these grains were intrinsically stagnant with regard to refinement during cryogenic rolling.

4. Summary

High-resolution EBSD was applied to examine grain structure development during cryogenic rolling of Cu–29.5Zn brass. The main conclusions from this work are as follows.

(1) Grain refinement was primarily related to deformation twinning and shear banding. The more typical grain-subdivision process associated with the development of dislocation boundaries was very limited. The latter behavior was attributed to low stacking fault energy and the cryogenic temperature, both of which suppressed climb and cross slip.

(2) Microstructure evolution was found to be broadly similar to that occurring during rolling at room temperature. At very low reductions, a series of low-angle dislocation boundaries aligned with {111} plane traces were formed. After 30-pct. reduction (true strain 0.4), profuse twinning was observed in grains having crystallographic orientations close to Copper {112}<111> and S {123}<634>. Once activated, twinning continued to 90 pct. reduction (true strain 2.3). Subsequent slip in the twinned areas produced a {111}<uvw> γ fiber texture. After 50-pct. reduction (true strain 0.7), extensive shear banding developed in the twinned areas which rotated the γ fiber toward Goss {110}<100> and Brass {110}<112> orientations. Shear banding gave rose to marked microstructure refinement, eventually producing a mean grain size of 0.2 μm.

(3) Grains with crystallographic orientations close to the Brass and Goss orientations were found to be stable against twinning/shear banding and thus underwent no significant grain refinement. As a result, the final

structure developed in heavily-rolled material was distinctly inhomogeneous consisting of coarse remnants of original grains with poorly developed substructure and ultra-fine grain domains.

(4) The decrease of the rolling temperature to the cryogenic range shifted the onset of twinning and shear banding to lower strains but was unable to activate these two mechanisms in grains with the Brass and Goss orientations. As a result, cryogenic rolling did not lead to the formation of a homogeneous ultra-fine grain microstructure.

Acknowledgements

Financial support from the Russian Fund of Fundamental Research (project No. 14-02-97004) is gratefully acknowledged. The authors are grateful to P. Klassman for technical assistance during cryogenic rolling.

Appendix A. Supplementary material

Supplementary data associated with this article can be found, in the online version, at http://dx.doi.org/10.1016/j.jallcom.2014.12. 241.

References

[1] Y. Huang, P.B. Prangnell, The effect of cryogenic temperature and change in deformation mode on the limiting grain size in a severely deformed dilute aluminum alloy, Acta Mater. 56 (2008) 1619–1632.

[2] T. Konkova, S. Mironov, A. Korznikov, S.L. Semiatin, Microstructural response of pure copper to cryogenic rolling, Acta Mater. 58 (2010) 5262–5273.

[3] S.V. Zherebtsov, G.S. Dyakonov, A.A. Salem, V.I. Sokolenko, G.A. Salishchev, S.L. Semiatin, Formation of nanostructures in commercial-purity titanium via cryorolling, Acta Mater. 61 (2013) 1167–1178.

[4] K.P. Sushanta, R. Jayaganathan, A study of the mechanical properties of cryorolled Al–Mg–Si alloy, Mater. Sci. Eng. A480 (2008) 299–305.

[5] K.P. Sushanta, R. Jayaganathan, V. Chawla, Effect of cryorolling on microstructure of Al–Mg–Si alloy, Mater. Lett. 62 (2008) 2626–2629.

[6] Y.S. Li, N.R. Tao, K. Lu, Microstructural evolution and nanostructure formation in copper during dynamic plastic deformation at cryogenic temperatures, Acta Mater. 56 (2008) 230–241.

[7] Y. Zhang, N.R. Tao, K. Lu, Mechanical properties and rolling behaviors of nanograined copper with embedded nano-twin bundles, Acta Mater. 56 (2008) 2429–2440.

[8] A.M. Hodge, Y.M. Wang, T.W. Barbee, Mechanical deformation of high-purity sputter deposited nano-twinned copper, Scripta Mater. 59 (2008) 163–166.

[9] Y. Estrin, N.V. Isaev, S.V. Lubenets, S.V. Malykhin, A.T. Pugachov, V.V. Pustovalov, E.N. Reshetnyak, V.S. Fomenko, S.E. Shumilin, M. Janecek, R.J. Hellmig, Effect of microstructure on plastic deformation of Cu at low homologous temperatures, Acta Mater. 54 (2006) 5581–5590.

[10] V. Subramanya Sarma, K. Sivaprasad, D. Sturm, M. Heilmaier, Microstructure and mechanical properties of ultra fine grained Cu–Zn and Cu–Al alloys produced by cryorolling and annealing, Mater. Sci. Eng. A489 (2008) 253–258.

[11] G.H. Xiao, N.R. Tao, K. Lu, Microstructures and mechanical properties of a Cu– Zn alloy subjected to cryogenic dynamic plastic deformation, Mater. Sci. Eng., A 513–514 (2009) 13–21.

[12] J. Das, Evolution of nanostructure in a-brass upon cryorolling, Mater. Sci. Eng. A530 (2011) 675–679.

[13] J. Hirsch, K. Lucke, M. Hatherly, Overview No. 76: mechanism of deformation and development of rolling textures in polycrystalline f.c.c. metals – III. The influence of slip inhomogeneities and twinning, Acta Metall. 36 (1988) 2905– 2927.
[14] H. Miura, T. Sakai, S. Maruoka, J.J. Jonas, Production of recrystallized nanograins in a fine-grained Cu–Zn alloy, Phil. Mag. Ltr. 90 (2010) 93–101.
[15] B. Roy, N.K. Kumar, P.M.G. Nambissan, J. Das, Evolution and interaction of twins, dislocations, and stacking faults in rolled a-brass during nanostructuring at sub-zero temperature, AIP Adv. 4 (2014) 067101.
[16] N.K. Kumar, B. Roy, J. Das, Effect of twin spacing, dislocation density, and crystallite size on the strength of nanostructured a-brass, J. Alloys Comp. 618 (2015) 139–145.
[17] K. Sekine, J. Wang, Characteristic features of rolling texture development in FCC alloys having very low stacking fault energies, Mater. Trans. 40 (1999) 1–6.
[18] Ye.V. Nesterova, V.V. Rybin, Mechanical twinning and fragmentation of technically pure titanium on developed plastical deformation stage, Phys. Met. Metall. 59 (1985) 395–406.
[19] W.Y. Yeung, A transition of microstructure in heavily cold rolled 70:30 brass, Scripta Met. 23 (1989) 617–620.
[20] A. Weidner, P. Klimanek, Shear banding and texture development in cold rolled a-brass, Scripta Mater. 38 (1998) 851–856.
[21] J. Tobisch, A. Mucklich, The development of rolling texture in a-brass determined by neutron diffraction, Texture 1 (1974) 211–231.
[22] F.J. Humphreys, M. Hatherly, Recrystallization and related phenomena, second ed., Elsevier, Oxford, 2004.

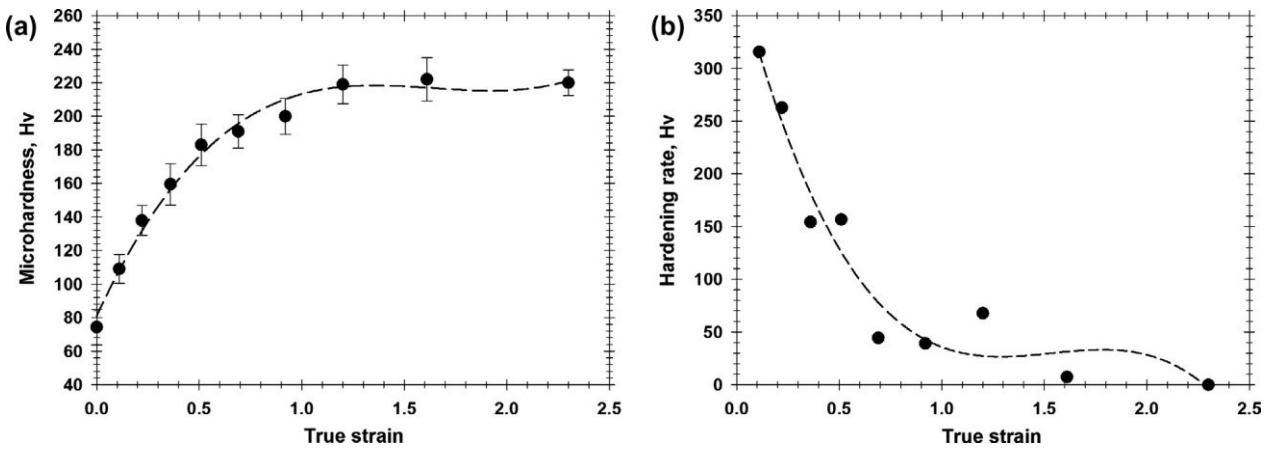

Fig. 1. Effect of true rolling strain on (a) mean microhardness and (b) hardening rate dH/de. dH and de denote the increment in microhardness and increment in true strain, respectively. In (a), error bars show the standard deviation of the measurements.

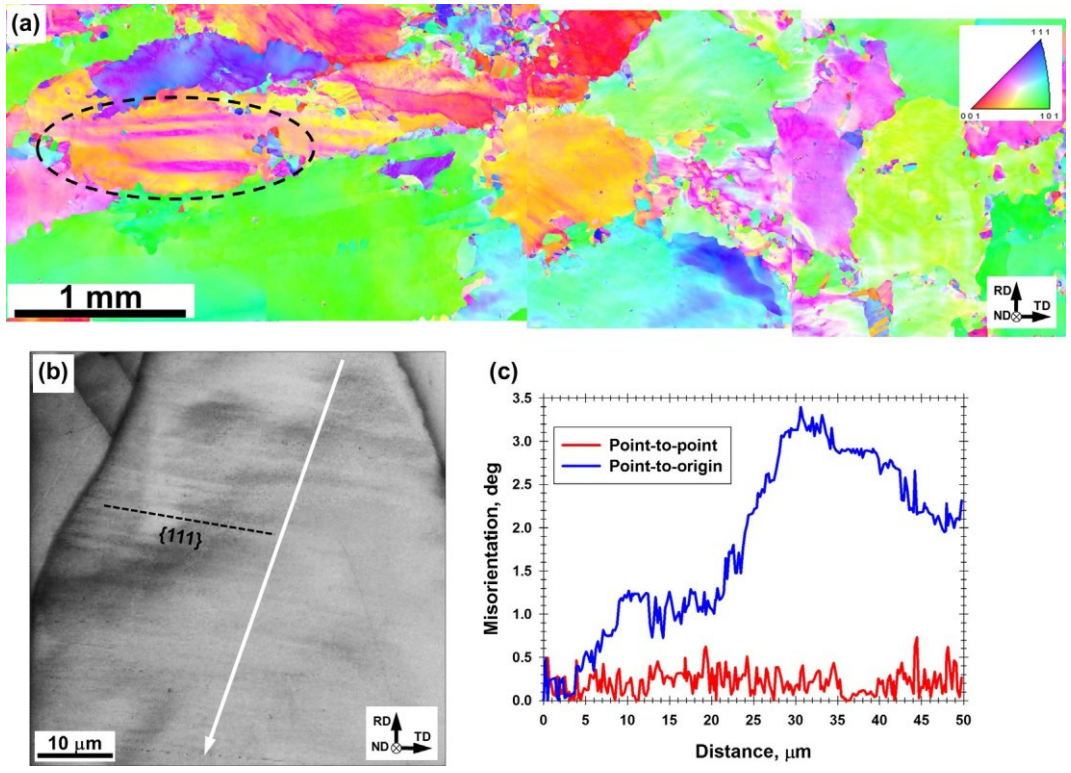

Fig. 2. Microstructure after 10-pct. thickness reduction (true strain of 0.1): (a) low-resolution, composite EBSD orientation map (color code triangle is given in the upper right corner), (b) high-resolution Kikuchi-band-contrast EBSD map, and (c) misorientation profile measured along the white line in (b). The circled area in (a) exemplifies grain splitting; the broken line in (b) shows the {111} plane trace closest to the deformation-induced boundaries.

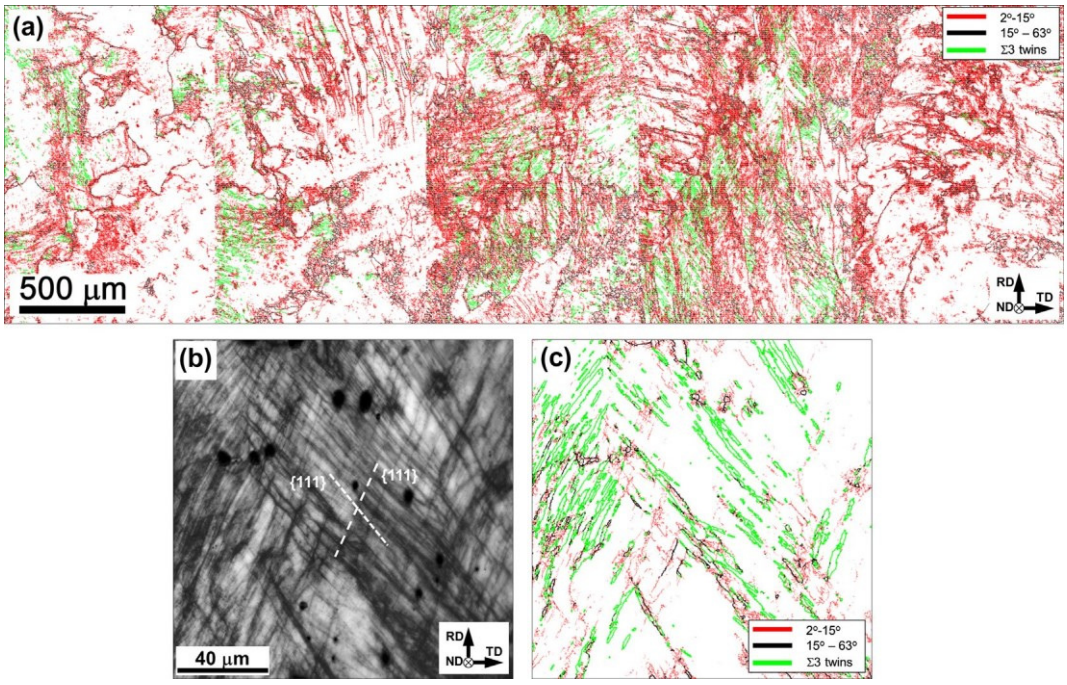

Fig. 3. Microstructure after 30-pct. thickness reduction (true strain of 0.4): (a) low-resolution, composite EBSD grain-boundary map (grain-boundary color code is given in the upper right corner), (b) high-resolution Kikuchi-band-contrast EBSD map taken from the twinned area, and (c) grain-boundary EBSD map from the same location as (b). The broken lines in (b) show the {111} plane traces closest to the twin habit planes.

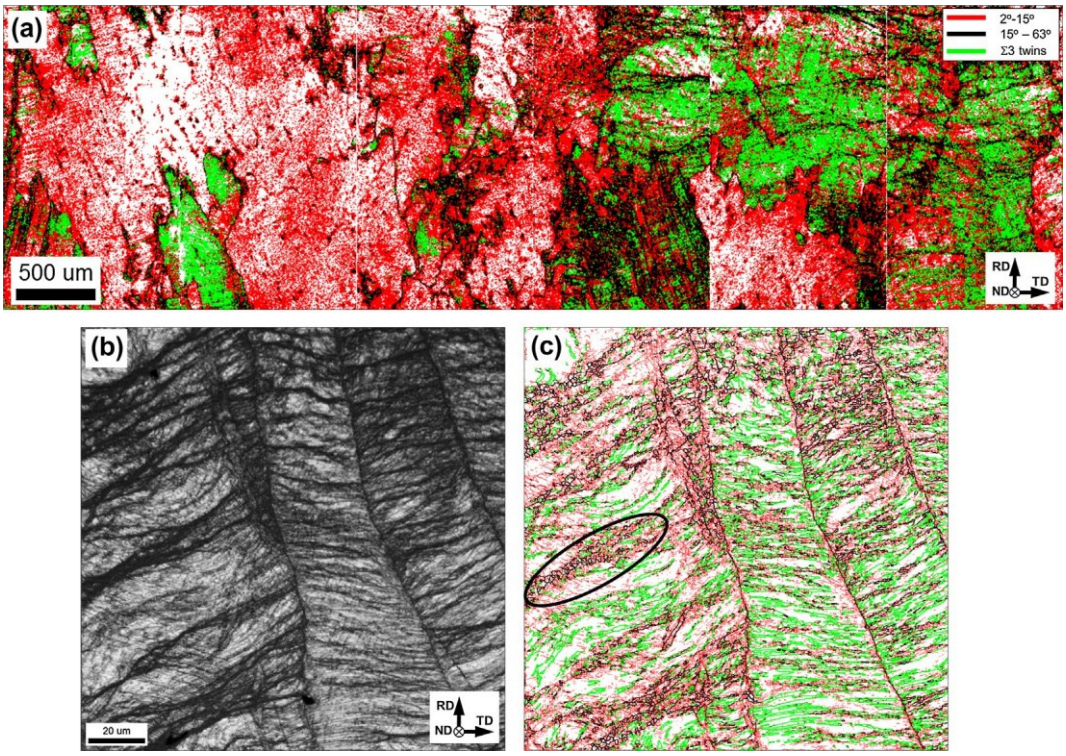

Fig. 4. Microstructure after 50-pct. thickness reduction (true strain of 0.7): (a) low-resolution, composite EBSD grain-boundary map (grain-boundary color code is given in the upper right corner), (b) high-resolution Kikuchi-band-contrast EBSD map illustrating shear banding, and (c) grain-boundary EBSD map from the same location as (b). The dark bands in (b) are shear bands; the circled area in (c) illustrates substructure within the bands.

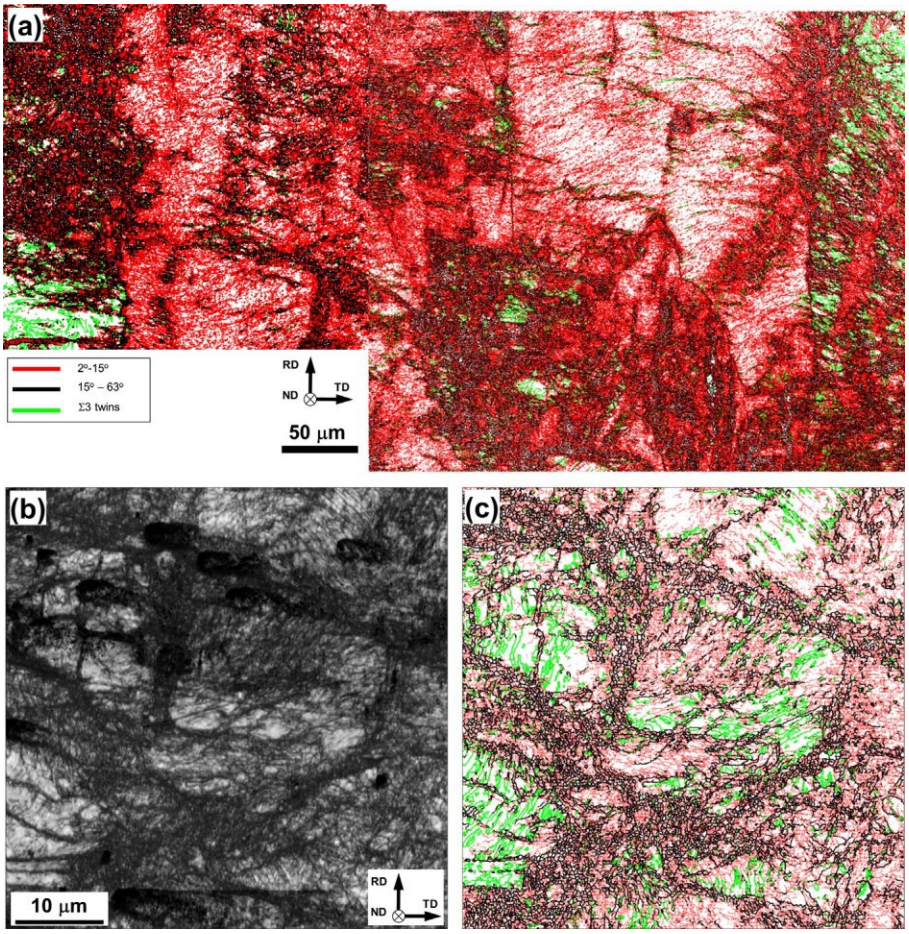

Fig. 5. Microstructure after 90-pct. thickness reduction (true strain of 2.3): (a) low-resolution composite EBSD grain-boundary map (grain-boundary color code is given in the lower left corner), (b) high-resolution Kikuchi-band-contrast EBSD map, and (c) grain-boundary EBSD map from the same location as (b).

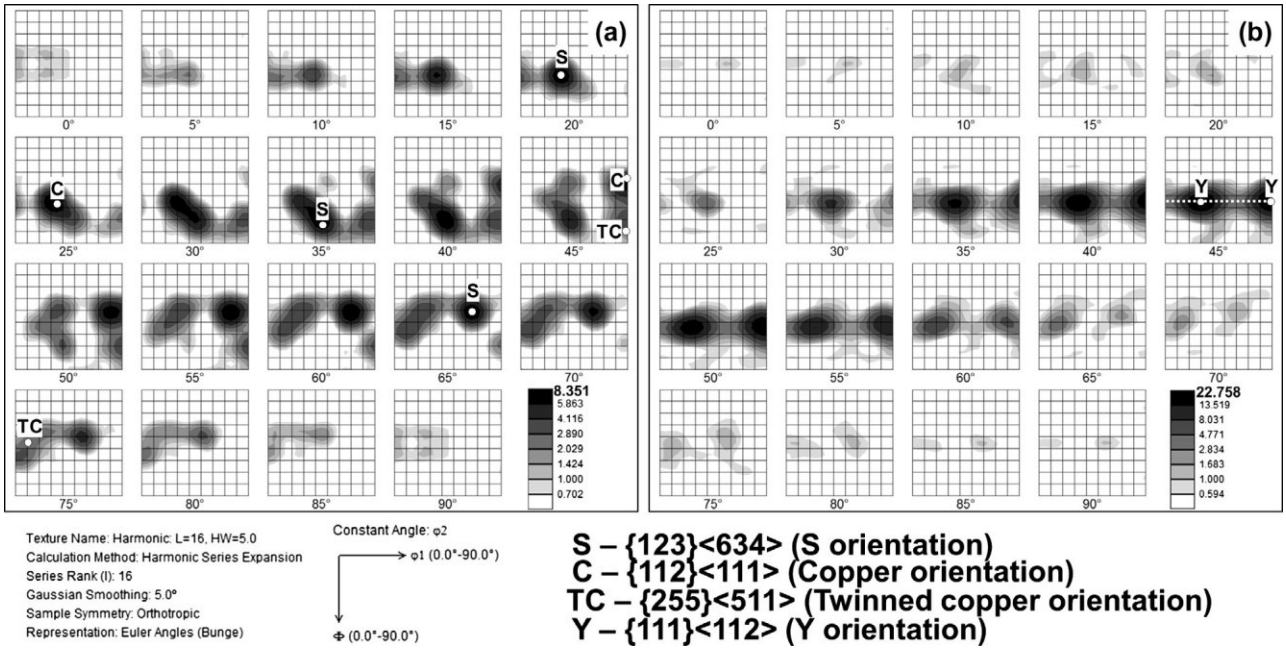

Fig. 6. Orientation-distribution functions (ODFs) for the crystallographic orientations of the twinned areas after a thickness reduction of (a) 50-pct. (true strain of 0.7) or (b) 90 pct. (true strain of 2.3). For comparison purposes, several ideal rolling orientations are superimposed on the ODFs. In (b), the broken line indicates the {111}<uvw> γ fiber texture.

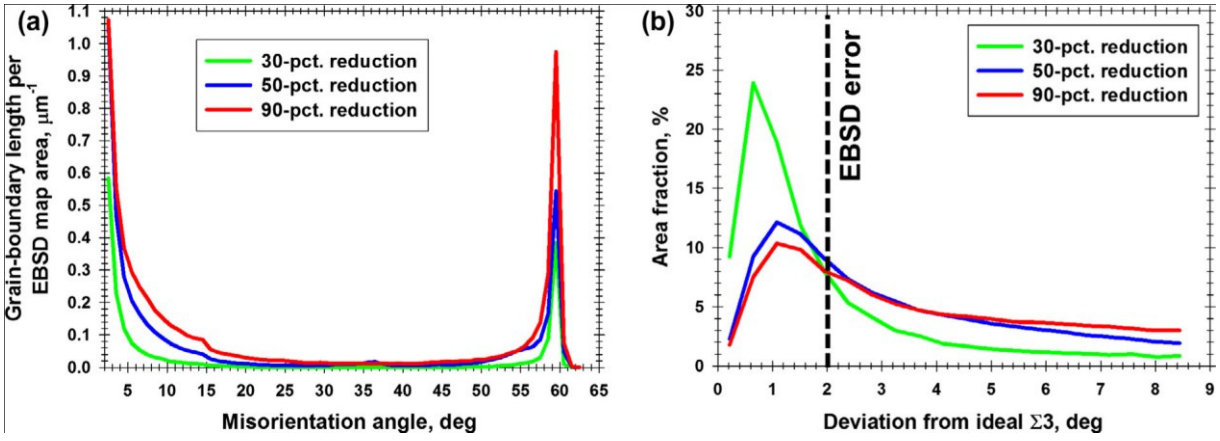

Fig. 7. Misorientation measurements in twinned areas: (a) Effect of rolling reduction on the misorientation-angle distribution and (b) the deviation of measured twin misorientations from the ideal Σ3.

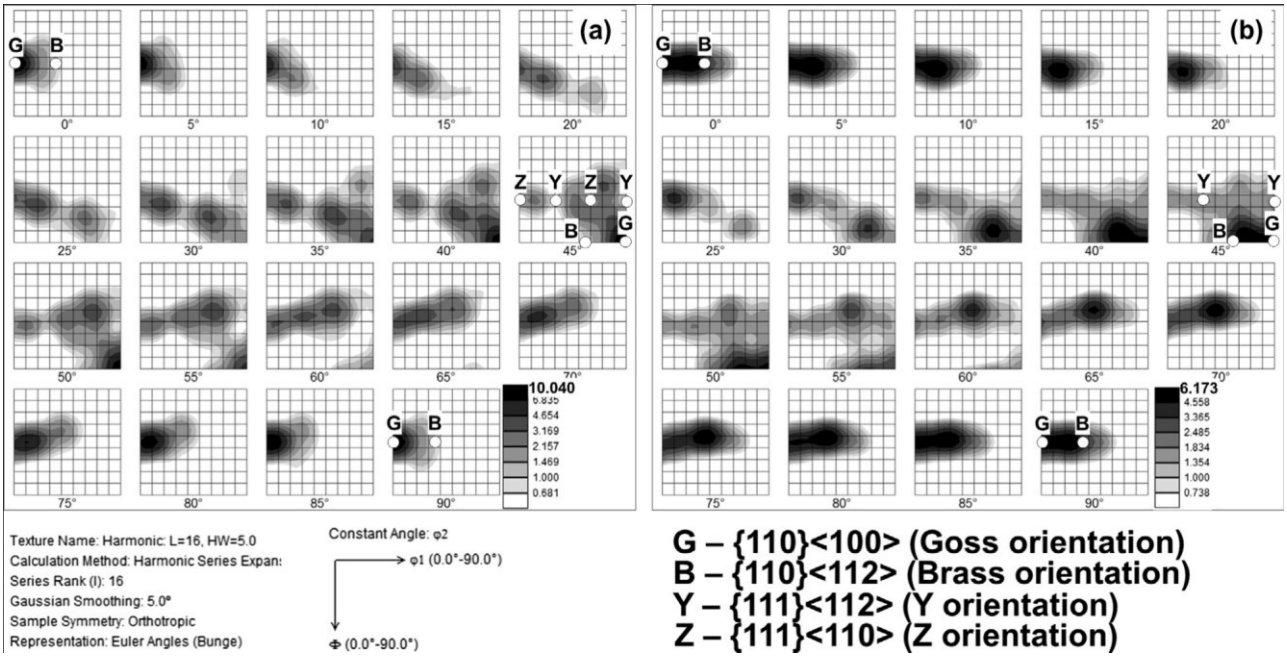

Fig. 8. ODFs for the crystallographic orientations within shear bands after a thickness reduction of (a) 60 pct. (true strain of 0.9) or (b) 90 pct. (true strain of 2.3). For comparison purposes, several ideal rolling orientations are superimposed on the ODFs.

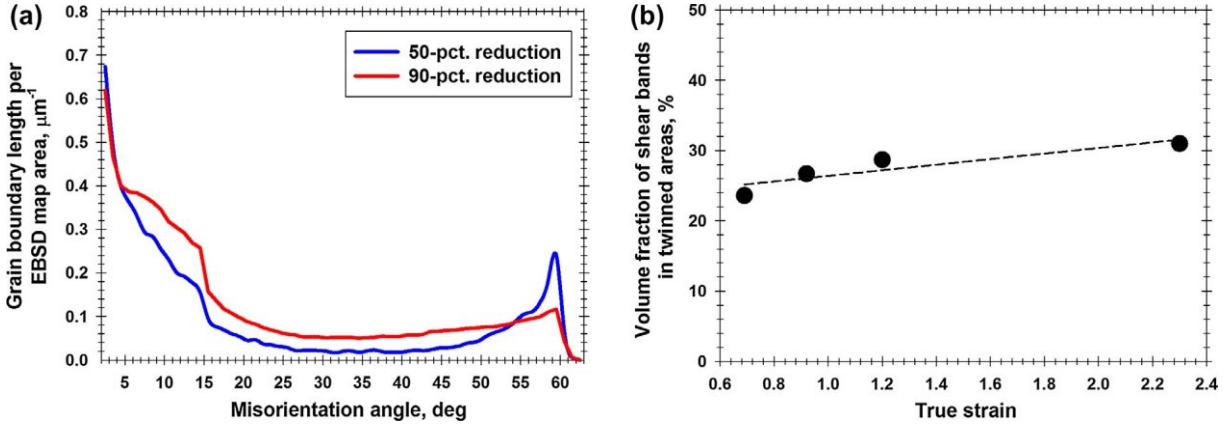

Fig. 9. Effect of thickness reduction on shear band development: (a) Misorientation-angle distribution and (b) volume fraction (within twinned areas).

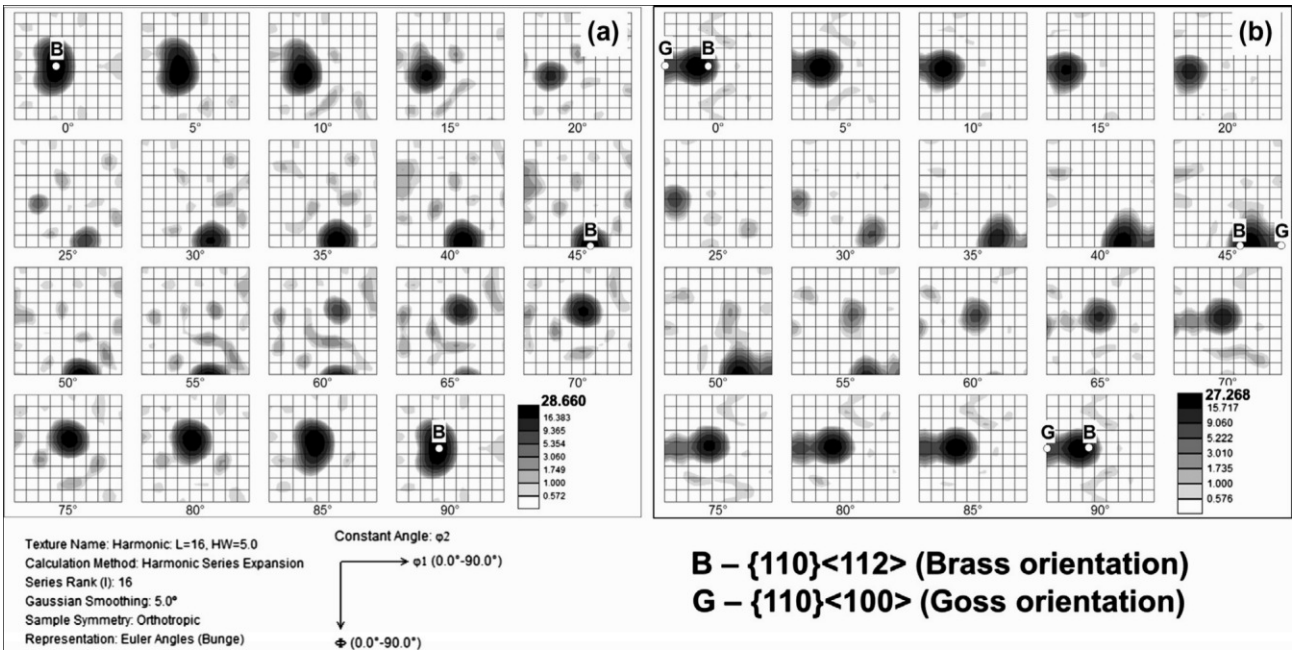

Fig. 10. ODFs for the crystallographic orientations of large remnant grains after a thickness reduction of (a) 50 pct. (true strain of 0.7) or (b) 90 pct. (true strain of 2.3). For comparison purposes, several ideal rolling orientations are superimposed on the ODFs.